Acta Cryst. (1987). B43, 97-106

Analysis of the Diffuse Scattering from Disordered Molecular Crystals: Application to 1,3-Dibromo-2,5-diethyl-4,6-dimethylbenzene at 295 K

BY T. R. WELBERRY AND J. SIRIPITAYANANON

Research School of Chemistry, Australian National University, PO Box 4, Canberra City, ACT 2601, Australia

(*Received* 26 *March* 1986; *accepted* 1 *September* 1986)

Abstract

The disorder diffuse X-ray scattering (DDS) in 1,3-dibromo-2,5-diethyl-4,6-dimethylbenzene, $C_{12}H_{16}Br_2$ (BEMB2), has been analysed using the least-squares procedure of Epstein & Welberry [*Acta Cryst.* (1983), A39, 882-892]. Data from seven reciprocal-lattice sections were used to obtain values for all intermolecular correlation coefficients within a 20 Å neighbourhood. Of the 42 correlations within this neighbourhood, 22 were found to be significantly different from zero, and of these 13 were significant at the 3σ level. The largest correlation of 0·21 was between a central molecule and the nearest neighbour in the [100] crystal direction. The five largest correlations were all of opposite sign to the corresponding correlations in the previously reported isostructural BEMB1 [Welberry & Siripitayananon (1986). *Acta Cryst.* B42, 262-272]. As for BEMB1, the observed correlations do not fully support a previously held theory that the short-range order occurs in such a way as to reduce the number of Br–Br intermolecular contacts in favour of CH_3–Br contacts. An unusual diffraction effect in which the diffuse scattering shows a deep depression of intensity close to the (010) reciprocal position has been observed. The origins of this feature, which is considered to arise from an analogous effect to the 'space-group absences' of conventional Bragg-peak data, are discussed.

1. Introduction

In a previous paper (Welberry & Siripitayananon, 1986) we have described the analysis of the disorder diffuse scattering in 1,4-dibromo-2,5-diethyl-3,6-dimethylbenzene (BEMB1) using the least-squares procedure described by Epstein & Welberry (1983). In the present paper we report a similar study of the diffuse scattering in the isomeric compound 1,3-dibromo-2,5-diethyl-4,6-dimethylbenzene (BEMB2). The average crystal structures for both these compounds obtained by conventional analysis of Bragg reflection data were reported by Wood, Welberry & Puza (1984). This work revealed that both compounds formed disordered crystals and that these were almost exactly isostructural. The disorder arises because each molecule is able to take up either of two different orientations at each molecular site in the crystal (see Fig. 1). To a good approximation the methyl C and Br atomic sites appeared disordered while the remaining diethylbenzene fragment of the molecule remained quite ordered. The only major difference between the two crystal structures was the different site occupancies obtained for the two alternative molecular orientations. For BEMB1 the two alternatives occurred with frequencies 0·56 and 0·44 while for BEMB2 the proportions were almost exactly equal.

In the diffuse scattering experiment we can obtain information concerning the mutual orientation of neighbouring molecules. We seek to determine values for correlation coefficients, $C_{n,m}$, for all intermolecular vectors within a given neighbourhood of a particular molecule. Here $C_{n,m} = (P_{AA} - m_A^2)/m_A m_B$ where P_{AA} is the joint probability that both sites n and m are occupied by molecules of the same type (orientation) A, and m_A and m_B are site occupancies. The analysis is carried out using so-called *random-* and *correlation-distribution* functions as basis functions in a least-squares procedure which establishes the values of the $C_{n,m}$ giving the best fit to the observed data. For further details of the procedure we refer the reader to Epstein & Welberry (1983) and Welberry & Siripitayananon (1986).

The diffuse scattering data used in these experiments is obtained from long-exposure Weissenberg photographs taken with the crystal mounted about a number of different axes. Since the data thus initially

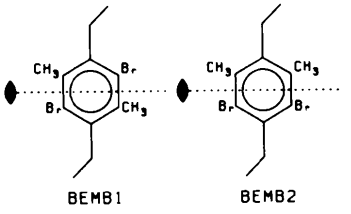

Fig. 1. Comparison of the molecular structure of BEMB1 and BEMB2. For each molecule, the alternative orientation which gives rise to the possibility of disorder may be obtained from that shown by a rotation through 180°, as indicated. (Note this requires a reorientation of the ethyl substituents.)

0108-7681/87/010097-10$01.50

consist of a number of two-dimensional (2D) reciprocal sections, two different approaches to the analysis have been used. In the first '2D method', each 2D section is analysed separately and then a set of simultaneous equations must be solved to obtain values for the three-dimensional $C_{n,m}$ values. In the second '3D method' the individual sections are first scaled together and the analysis then carried out in three dimensions. For further details of these approaches see Welberry & Siripitayananon (1986).

In the present paper we rely heavily on experimental and theoretical results established in previous papers, and for the sake of brevity details of these are not reproduced, except where necessary for the present argument. In particular, frequent reference is made to the previous study (Welberry & Siripitayananon, 1986) of BEMB1 which hereafter is simply referred to by name.

2. Data collection

Long-exposure (~3 d) Weissenberg photographs were taken at room temperature (295 K) of the same five reciprocal-lattice sections ($h0l$, $hk0$, $0kl$, $hk\bar{h}$ and $hk2\bar{h}$) as used for the previous BEMB1 analysis, using a conventional 28·65 mm radius Weissenberg camera with a layer-screen gap width of 1 mm and graphite-monochromated Cu $K\alpha$ radiation. Although it was necessary to use different crystals for each mounting and individual sections were recorded at various times over a period of several months, spherical solution-grown (from PE) crystals of −0·5 mm diameter were used in each case. To aid in preliminary investigations and for later reference, these photographs were digitized and the data processed in the manner described by Welberry & Jones (1980) to produce the undistorted views of each reciprocal section which are shown in Fig. 2. For quantitative intensity measurements, individual densitometer readings were made directly from the Weissenberg films on the same grid of $a^*/10$, $b^*/20$ and $c^*/5$ as previously used for BEMB1. The cell data are given in Table 1. Both halves of the Weissenberg films were measured in the range $2{\cdot}5 < \theta < 25{\cdot}6°$ and after an empirical background correction was applied to the data using the procedure described by Welberry & Glazer (1985), symmetry-related data were averaged. The number of data recorded for each section is given in Table 2.

The $h0l$ reciprocal section shown in Fig. 2 shows a marked contrast to the corresponding section of BEMB1. Whereas in BEMB1 most of the diffuse scattering appeared in regions well removed from Bragg peaks, here the strongest regions appear near to Bragg peaks and consequently are not easily distinguished from thermal diffuse scattering (TDS). For this reason it was decided at a later stage to collect data from the reciprocal-lattice sections $h\frac{1}{2}l$ and $h\frac{1}{4}l$ which provide additional information of the structure

Table 1. *BEMB2 cell data and average structural information assuming space group $P2_1/c$*

$a = 9{\cdot}088$, $b = 4{\cdot}444$, $c = 17{\cdot}970$ Å, $\beta = 122{\cdot}69°$.

	Coordinates for Br and C(methyl) for molecule in orientation A (Site occupancy $m_A = 0{\cdot}5$)			Coordinates for Br and C(methyl) for molecule in orientation B (Site occupancy $m_B = 0{\cdot}5$)		
	x	y	z	x	y	z
Br(1)	0·2213	0·2493	0·0462	0·0900	0·6182	−0·1306
Br(2)	0·9100	0·3818	0·1306	0·7787	0·7507	−0·0462
C(1)	0·0900	0·6182	−0·1306	0·2213	0·2493	0·0462
C(2)	0·7787	0·7507	−0·0462	0·9100	0·3818	0·1306

To calculate the distribution functions we specify the molecular site 55501 as (x, y, z) and the site 55502 as $(x, \frac{1}{2}-y, \frac{1}{2}+z)$.

projected down the **b** axis. These data were collected from equi-inclination Weissenberg photographs using a cylindrical crystal of diameter ~0·6 mm shaped using the crystal grinder reported by Wood, Tode & Welberry (1985). Without the presence of Bragg peaks the alignment of these films on the densitometer was achieved by superposing the films on the corresponding zero-level photograph and making use of the same alignment parameters as for that photograph.

For each section, all data suspected of being attributable to TDS were removed by the same selection procedures described for BEMB1. The regions of data accepted for use in the subsequent analysis are shown in Fig. 2 alongside the corresponding reciprocal-lattice sections. Note that, for $h0l$, regions around many Bragg peaks have been removed which subsequent analysis revealed were not TDS but actually part of the disorder diffuse scattering (DDS). The number of accepted data for each section is given in Table 2.

3. Data analysis

Like BEMB1, BEMB2 crystallizes in space group $P2_1$ but the departures from the more symmetric space group $P2_1/c$ are very small (see Wood, Welberry & Puza, 1984). This means that, if the space group $P2_1$ is used in the diffuse scattering analysis, the correlation distributions that are calculated for molecular sites which are symmetry related in $P2_1/c$ but unrelated in $P2_1$ are still virtually identical, and the least-squares matrix used in the analysis is very ill-conditioned. Consequently it was necessary to perform the analysis in the more symmetric space group $P2_1/c$. As was the case for BEMB1, a structure refinement in $P2_1/c$ was also available for BEMB2 (Jones, Welberry & McLaughlin, unpublished) and the atomic coordinates of the disordered Br and methyl C atom sites used in the calculation of the correlation distributions are given in Table 1. It will be noticed that the coordinates for each Br position in molecule A are the same as those for the C(methyl)

Table 2. *Details of the least-squares analyses for BEMB2*

	Reciprocal-space section						
	$0kl$	$h0l$	$hk0$	$hk\bar{h}$	$hk2\bar{h}$	$h\frac{1}{4}l$	$h\frac{1}{2}l$
Number of accepted data	1154	2340	1445	1587	1286	2976	3463
Number of excluded data	527	989	242	437	480	342	31
Number of distributions, x_l in 2D refinement	13	9	28	22	26	14	5
Background constant, c_{2D}	5·5	7·8	5·2	2·6	5·5	2·6	3·8
Background constant, c_{3D}*	3·3	7·8	6·5	3·2	5·4	2·3	4·8
Agreement factors (2D)							
$R=[\sum(I_o-I_c)^2/\sum(I_o)^2]^{1/2}$	0·45	0·33	0·38	0·30	0·30	0·32	0·28
$R_{real}=[\sum(I_o-I_c)^2/\sum(I_o-c_{2D})^2]^{1/2}$	0·55	0·44	0·45	0·39	0·36	0·42	0·34
Agreement factors (3D)							
$R=[\sum(I_o-I_c)^2/\sum(I_o)^2]^{1/2}$	0·49	0·34	0·40	0·32	0·32	0·35	0·29
$R_{real}=[\sum(I_o-I_c)^2/\sum(I_o-c_{3D})^2]^{1/2}$	0·55	0·45	0·48	0·45	0·38	0·44	0·37
Scale factors for 3D analysis	1·0	0·6	0·8	2·3	1·0	1·0	1·0

* Note that these 3D constants have been adjusted to correspond to the original scale of each 2D section of data.

positions of molecule *B*, and *vice versa*. More correctly the C(methyl) should be closer to and the Br somewhat further away from the central ring than these refined composite positions, but preliminary calculations showed that for the low-θ range used in the experiment differences resulting from this approximation were negligible. In calculating these distributions, to be used in the least-squares analysis, an isotropic temperature factor corresponding to a mean-square atomic displacement of 0·06 Å^2 was used throughout. We adopted this isotropic value since the anisotropic parameters obtained in the structure refinement refer to composite disordered atoms and do not truly reflect the thermal motion of an individual atom.

In space group $P2_1/c$ the molecular site has a centre of symmetry and, since the BEMB2 molecule does not, this necessarily means that the site occupancy for BEMB2 must be 0·50. In $P2_1$ this restriction no longer applies but it is interesting to note that in the $P2_1$ refinement of Wood *et al.* (1984) the site occupancy differed from 0·5 only in the third decimal place. It should also be noted that the asymmetric unit in $P2_1/c$ is only half of one molecule and since we need to use a whole molecule as the basic unit in the calculation only two equivalent-position specifiers are required to specify the different molecular sites. With the usual *ORTEP*II (Johnson, 1976) method of site labelling the two specifiers chosen were (x, y, z) for the site 55501 and $(x, \frac{1}{2}-y, \frac{1}{2}+z)$ for 55502. With this notation the label 56501, for example, refers to the molecule at $(x, 1+y, z)$ and (66502) to that at $(1+x, \frac{3}{2}-y, \frac{1}{2}+z)$.

Correlation distributions were calculated for all molecular sites within a neighbourhood of 20 Å of a particular site. With the assumption that the same correlation will exist along symmetry-related vectors the number of distinct correlation distributions was reduced from 112 to 42. Site labels for these 42 distributions, together with their symmetry equivalents, may be found in the table of final $C_{n,m}$ values (Table 3). The choice of 20 Å for the extent of the neighbourhood outside which correlations are assumed to be negligibly small is dictated by two factors. Firstly, the resolution of the recorded diffuse patterns is limited by the gap width of the Weissenberg layer screens (see Welberry, 1983). For a 1 mm gap, diffuse fringes corresponding to real-space vectors greater than ~50 Å will not be resolved over the whole 2·5–25·6° θ range which is used in the analysis. 20 Å represents a convenient cut-off for vectors giving distribution functions which will be well resolved over the whole area of reciprocal space covered by the present data. In addition the use of further shells of neighbouring molecules would introduce an unmanageable number of additional correlation functions.

3.1. *Individual section analyses*

Individual 2D sections were analysed using the least-squares procedure of Epstein & Welberry (1983), in the same manner as described for BEMB1. The number of distribution functions used for each section together with various statistics obtained from these analyses are shown in Table 2. Comparison of these results with the corresponding results for BEMB1 shows that the agreement factors are generally higher in BEMB2. Agreement for the $0kl$ section is particularly poor. For this section a plot of the minimum intensity occurring in each $\sin(\theta)$ range for the *random* distribution revealed a large peak between approximately $\theta=5$ and 12°. This would undoubtedly mean that the empirical background correction which is applied to the data (see Welberry & Glazer, 1985) would be a poor approximation to the true background in this case, since it assumes that in each 1° range of θ the scattering will be close to zero at some value of ω, the crystal orientation. For each of the other sections similar plots revealed the approximation to be good and for these no particular problems with the empirical correction should be anticipated. Consequently, although part of the particularly high R value for the $0kl$ section is probably attributable to the poor background correction, the

generally high values for all of the other sections when compared to the corresponding ones for BEMB1 require further explanation.

A second aspect of the 2D analyses which differed substantially from the BEMB1 case was that the least-squares matrices revealed that many more of the 2D distribution functions were highly correlated. This was particularly true for the $(hk2\bar{h})$ section where there were ~60 elements of the correlation matrix with values in excess of 0·8. For BEMB1 some prob-

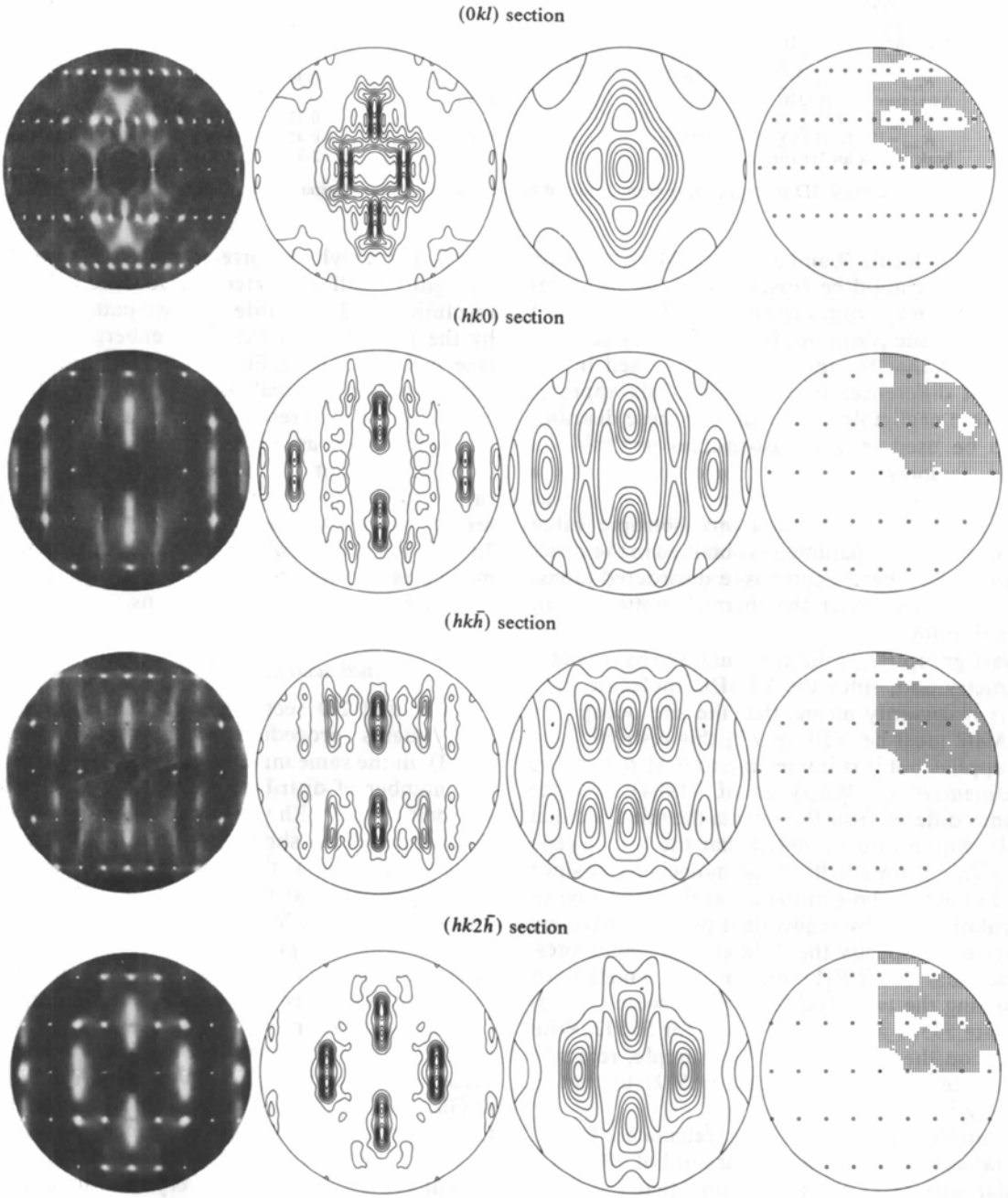

Fig. 2. Observed and calculated diffuse scattering intensities for the seven reciprocal sections used for BEMB2. The leftmost column shows the undistorted photographic images of the observed X-ray data for each section. The second column shows contour plots of the intensity in the corresponding section, calculated from the final $C_{n,m}$ given in Table 3. The third column shows comparison contour plots of the calculated intensity corresponding to the case if all correlations were zero (the random distribution). The rightmost column indicates the points in each section at which the intensities used in the least-squares analysis were measured. For sections $(0kl)$, $(hk0)$, $(hk\bar{h})$ and $(hk2\bar{h})$, $\mathbf{b}^*$ is vertical; for sections $(h0l)$, $(h\frac{1}{4}l)$ and $(h\frac{1}{2}l)$, $\mathbf{c}^*$ is horizontal.

lems of this kind were encountered but it was possible to overcome them simply by omitting from the solution procedure the problematical distribution coefficients. In the present case when the equations involving all such highly correlated distribution coefficients were eliminated from the set of simultaneous equations used to solve for $C_{n,m}$, the number of equations remaining proved insufficient to allow a solution. Consequently it became necessary to abandon the 2D analysis method and use only the 3D analysis technique.

3.2. 3*D analysis*

The difficulties in obtaining scale factors for the individual sections of data in a situation where few common data points exist, where each section is likely to contain a different amount of residual background, and where the intrinsic accuracy of the data is likely to be fairly low, were discussed in the context of the BEMB1 analysis. For BEMB2, despite the fact that additional reciprocal sections were recorded, similar difficulties were encountered and no completely satisfactory means of directly scaling the data was found. However it was found possible for approximate scale factors to be established by comparing the peak intensities of certain strong peaks which occurred on more than one section. For example, the strong diffuse peak extending between the reciprocal points $0, \frac{1}{2}, 0$ and $0, \frac{3}{2}, 0$ is intersected by the four reciprocal sections $0kl$, $hk0$, $hk2\bar{h}$, $hk\bar{h}$ and this should in principle provide the means of obtaining an accurate estimate of the relative scales for these sections.

Reference to the undistorted photographs for these reciprocal sections (see Fig. 2), however, reveals that along the $0k0$ axis this peak appears quite different on the different sections. While in $(hk\bar{h})$ there appears to be a dark 'hole' associated with the 010 reciprocal point, for $0kl$ the intensity at the same point appears to be a maximum. We attribute this difference to the limitation of the resolution imposed by the use of the Weissenberg method, for which the resolution within

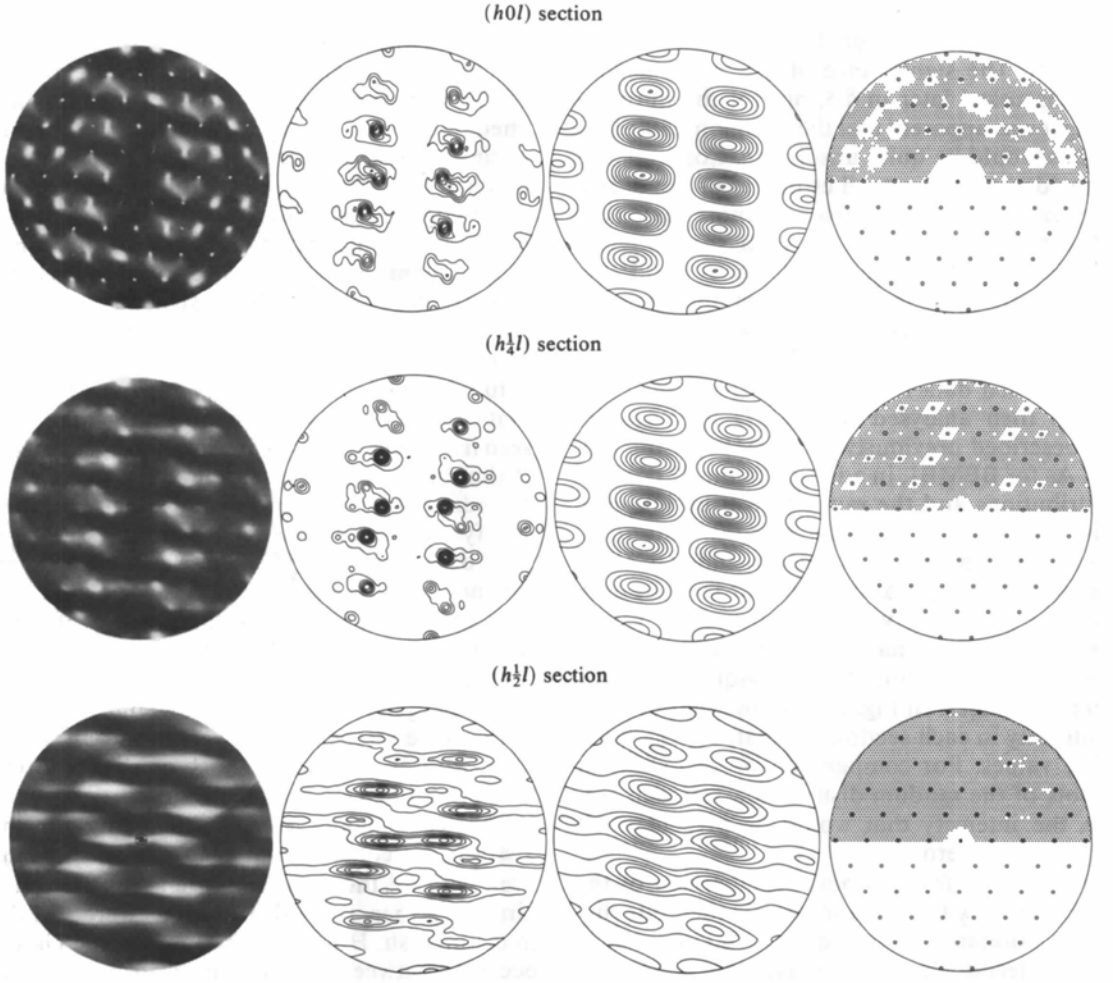

Fig. 2 (*cont.*)

Table 3. *Final results for the correlation coefficients, $C_{n,m}$, obtained from the 3D method of analysis*

$\bar{\sigma} = 3\sigma_{3D}$ is an estimate of the standard error based on analogy with the BEMB1 analysis. Only the 42 unique distribution codes are listed. For each 01-type code specified by the three integers (i, j, k) there is another symmetry-equivalent site with a designation code specified by $(10-i, 10-j, 10-k)$. For each 02-type code there are three additional symmetry-equivalent codes specified by $(i, 11-j, k)$; $10-i, j, 9-k)$; $(10-i, 11-j, 9-k)$.

Site	$C_{n,m}(\sigma_{3D})$	$\bar{\sigma}$	$C_{n,m}/\bar{\sigma}$	Site	$C_{n,m}(\sigma_{3D})$	$\bar{\sigma}$	$C_{n,m}/\bar{\sigma}$
65501	0·214 (7)	0·022	9·8	64601	0·026 (9)	0·027	1·0
66502	0·139 (5)	0·017	8·2	67402	−0·016 (6)	0·017	0·9
65601	0·098 (4)	0·012	8·0	69502	−0·014 (5)	0·016	0·9
57501	0·068 (4)	0·012	5·7	62501	−0·018 (9)	0·027	0·7
56502	0·084 (5)	0·016	5·2	67601	−0·026 (12)	0·035	0·7
56501	−0·102 (7)	0·020	5·2	58502	0·010 (6)	0·017	0·6
75601	0·059 (4)	0·012	5·0	66601	0·015 (9)	0·027	0·6
55601	0·049 (4)	0·012	4·2	76501	−0·014 (8)	0·023	0·6
64501	−0·121 (10)	0·031	3·9	67501	0·017 (10)	0·031	0·5
75501	0·046 (4)	0·012	3·9	56401	−0·012 (8)	0·023	0·5
66501	−0·103 (10)	0·031	3·3	77601	−0·014 (10)	0·031	0·5
76502	0·032 (3)	0·010	3·3	69501	0·010 (6)	0·019	0·5
66402	0·030 (3)	0·010	3·1	78502	−0·008 (6)	0·017	0·4
67502	−0·039 (5)	0·016	2·5	68502	0·006 (5)	0·015	0·4
58501	−0·041 (6)	0·019	2·1	59502	−0·005 (5)	0·015	0·3
57502	−0·035 (6)	0·017	2·0	63501	−0·009 (12)	0·035	0·3
77502	−0·023 (6)	0·017	1·3	76601	−0·008 (8)	0·023	0·3
56601	0·030 (8)	0·023	1·3	68501	−0·009 (9)	0·027	0·3
74501	−0·026 (8)	0·023	1·1	73601	−0·005 (10)	0·031	0·2
59501	0·018 (5)	0·016	1·1	68402	0·004 (6)	0·017	0·2
74601	0·026 (8)	0·023	1·1	63601	−0·006 (12)	0·035	0·2

a reciprocal section is different from that in a direction normal to it. The significance of this peak and the 'hole' is discussed later in § 5, but for the purposes of scaling it was apparent that the common data along the **b*** axis would be quite unsuitable. Consequently it was decided to use instead estimates of the diffuse peak intensities obtained from a more extensive region around the $0k0$ line on each section. As a result of this procedure, and similar ones applied to the intersections of other pairs of sections, approximate scale factors for all the reciprocal sections were obtained and these are given in Table 2.

The combined data from all seven reciprocal sections were then analysed by the 3D least-squares method described previously for BEMB1, using unit weights. As for BEMB1, in addition to the 42 correlation distributions and the random distribution used as basis functions for the least squares, additional *section-constant* functions were also included to allow refinement of the residual background level in each section. The resulting values of the $C_{n,m}$ values derived from this 3D analysis are given in Table 3, with e.s.d.'s derived from the least-squares matrix given in parentheses. In Fig. 2 we show contour plots of the intensity in each section calculated using these final $C_{n,m}$ values. For comparison we also show in Fig. 2 plots of the random distribution for each section, *i.e.* the intensity that would be present if all correlations were zero.

For BEMB1 we found from a comparison of the results obtained by the 2D and the 3D methods that the e.s.d.'s estimated from the least-squares matrix probably underestimate the true error by a factor of about three. Since the present experiment was similar to the BEMB1 case in every way, we would expect a similar factor to apply in the present case, but because of the failure of the 2D solution method no direct check on this is available. This underestimation occurs because the data are measured on a grid which is much finer than the rather broad features of most correlation distributions, and consequently measurements from adjacent points will not be completely independent. For further discussion of this effect we refer the reader to the BEMB1 paper. In Table 4 we have therefore assumed a value of $\bar{\sigma} = 3\sigma_{3D}$ and to assess the level of significance of individual $C_{n,m}$ values we list values of $C_{n,m}/\bar{\sigma}$. From this it is seen that 22 coefficients are significantly different from zero including 13 which are significant at the $3\bar{\sigma}$ level. It should be noted that although the $C_{n,m}$ are treated as independent variables in this analysis, they must satisfy certain consistency relations as discussed in § 2.4 of Welberry (1985). These relationships express the fact that, for example, if A is correlated to B and B is correlated to C, then there will of necessity be a correlation between A and C which must fall within certain limits. For high values of the correlations the limits are generally quite narrow, but for low values of the correlations they are very broad. In the present case, with all $C_{n,m}$ small, such consistency relations are certainly easily satisfied.

The least-squares correlation matrix for this 3D analysis did contain some high values, showing that, even with all the data from the seven sections combined together, some distributions were still difficult to distinguish. However, nearly all of the high values occurred between unimportant distributions that had $C_{n,m}$ values not significantly different from zero. The

Table 4. *Comparison of the strongest correlations in BEMB2 with the corresponding values in BEMB1*

The contact types and intermolecular distances (in Å) refer to a structure in which all molecules are in orientation *A*. Distances for BEMB2 are calculated using the coordinates of the composite disordered atomic site positions given in Table 1.

	$C_{n,m}$		Contact type	
Site	BEMB2	BEMB1	BEMB2	BEMB1
65501	0·21	−0·14	(Me–Br 4·08) (Me–Me, Br–Br 3·90)	(Br–Br 4·12) (Br–Me, Me–Br 3·91)
66502	0·14	−0·21	(Br–Me 4·29)	(Me–Me 4·24)
64501	−0·12	0·09	—	—
66501	−0·10	0·02	(Me–Br 4·08)	(Br–Br 4·10)
56501	−0·10	0·03	(Me–Br, Me–Br 3·90) (Me–Me, Br–Br 4·44)	(Me–Br, Br–Me 3·92) (Me–Me, Br–Br 4·45)

only two pairs of significant distributions which were correlated with coefficients greater than 0·5 were 56501/58501 with a coefficient of −0·73 and 64501/66501 with a coefficient of −0·62. In both these cases the presence of the correlation is reflected in the higher than average e.s.d.'s (see Table 3). This behaviour is in marked contrast to the effects encountered in the 2D analysis, where the difficulties in obtaining a solution for the $C_{n,m}$ arose because of the involvement in the correlation problems of many of the most significant distributions.

Some statistical details of the analysis are given in Table 2. The values of R_{real} show the level of agreement between observed and calculated intensities for each section within the 3D analysis, when the refined constant has been subtracted from the observed data. In general appearance the calculated patterns shown in Fig. 2 are in good agreement with the corresponding observed intensity distributions, particularly when the latter are compared to the patterns corresponding to zero correlation, but very close agreement is not borne out by the values for R_{real} given in Table 2 which in most cases are somewhat higher than the corresponding values for BEMB1. Since the experimental procedures and consequently the expected quality of the data were the same in the two experiments, this anomaly requires further explanation.

Although the 2D-analysis method was not able to yield a solution for the 3D $C_{n,m}$ values, we can compare the 2D analyses with the results for individual sections from the final 3D analysis. As a result we find that the solution afforded by the 3D method gives calculated intensities for the individual sections which agree with the observed intensities almost as well as did the individual section analyses. It was found in the case of BEMB1 that the individual 2D analyses were able to adjust to some extent to model features of the diffraction pattern which were not properly part of the DDS. The 3D analysis on the other hand is constrained by the necessity to model the DDS in all sections simultaneously and is not so easily able to model extraneous features of the pattern, and this results in the slightly higher R factors. The fact that the 3D solution gives agreement for individual sections almost as good as for each of the 2D section analyses suggests that the residual disagreement is attributable to systematic differences between the model and the data, and is not due to any failure to find a solution for the $C_{n,m}$ consistent with the different views of the diffuse scattering which the different mountings of the crystal provide. If the different sections were incompatible, whether because the scattering from the different crystals used was different or because there were significant errors in the section scale factors used, it might be expected that the agreement would be substantially worse for the 3D solution.

Detailed comparison of the observed and plotted patterns for the $0kl$ section shows that the very strong diffuse peaks elongated along $\mathbf{b}^*$ and occurring close to (010) and (002) are much narrower and more sharply peaked in the X-ray pattern than in the corresponding calculated pattern. The result of this is that at the centre of these peaks $I_{\text{obs}} > I_{\text{calc}}$ and conversely at their periphery $I_{\text{calc}} > I_{\text{obs}}$. Although over most of the section the diffuse scattering shows fairly broad peaks indicative of the low-order correlations that were revealed by the 3D analysis, the narrowness of these two peaks, particularly close to (010) and (002), is indicative of significant correlations existing at longer range, outside the chosen (20 Å) molecular environment. It simply is not possible to model these features with the distributions used since no functions with sufficiently high spatial frequencies were included in the analysis.

Similar considerations apply also to the dark 'hole' near (010) mentioned previously, which is apparent on $(hk0)$, $(hk\bar{h})$ and $(hk2\bar{h})$. Further discussion of this feature of the BEMB2 pattern is given in § 5. It suffices to say here that because the dimensions of the hole are a small fraction of the reciprocal-cell repeat distance, to model this feature satisfactorily would also require spatial frequencies much larger than any included in the current model, although the calculated patterns show that the least squares has attempted to model the feature to some extent, resulting in a depression in the diffuse intensity at the (010) point.

The above two examples serve to illustrate the fact that in BEMB2 it appears that there are significant contributions to the diffuse intensity from intermolecular vectors outside the chosen 20 Å molecular environment and this goes some way towards explaining the higher R factors obtained for BEMB2. It must be stressed, however, that for the distributions that *were* included in the analysis the experiment should provide good resolution over the whole area covered by the data. In this case, while the lack of inclusion of higher-order distributions involving the larger spatial frequencies may result in poor agreement factors, values obtained for the well resolved low-order

correlations should not be greatly affected. To test this we carried out some tests on a hypothetical intensity distribution which included known values of correlation coefficients of various orders. When the distribution was fitted with our least-squares program using only low-order distribution functions, the known correlation coefficients were retrieved to high accuracy even though the R factors obtained were high because of the missing functions. This result was obtained under a variety of conditions provided that the functions were fitted over a reasonably complete section of reciprocal space. Consequently in the BEMB2 experiment, in which every effort was made to cover reciprocal space as fully as possible within the limitations imposed by the necessity to eliminate TDS, we can be reasonably confident that the values of $C_{n,m}$ determined are reliable estimates of these parameters.

4. Results and discussion

A stereoplot of the structure of BEMB2 showing the environment of the molecule at site 55501 is shown in Fig. 3. All intermolecular contacts <4·5 Å between the disordered atomic sites are shown and these are indicated by dashed lines. In the figure, open circles represent C atoms, dark circles represent Br atoms, and all the molecules depicted are in orientation *A*. The four symmetry-related sites 55502, 56502, 55402 and 56402 are also in immediate contact with 55501 but only *via* their ordered ethyl substituents and these neighbours are omitted for clarity. In neither BEMB1 nor BEMB2 do the ethyl substituents seem to have any major effect on intermolecular correlations. It should be mentioned that, unlike in BEMB1, the ethyl substituents in BEMB2 are inequivalent, one being sandwiched between the two bromines and the other between the two methyls. No evidence for any significant difference in conformation of the two ethyls was detected in the crystal-structure determination, however, and to a good approximation the ethyl groups must be assumed to remain in the same position irrespective of the particular molecular orientation (*A* or *B*) and hence should not affect the short-range ordering.

In discussing the values of correlations observed along different intermolecular vectors it is interesting to make a comparison between the results for BEMB2 from this study with those previously obtained for BEMB1. In Table 4 we list the sites having the largest values of $C_{n,m}$ for BEMB2 together with the corresponding values from the BEMB1 study. A number of similarities and differences between BEMB1 and BEMB2 are clearly brought out in this table:

(i) The three strongest correlations in both cases are between the molecule at 55501 with those at 65501, 66502 and 64501, although the order of these is not the same.

(ii) These three correlations and those for the next two largest correlations, also listed, are however of *opposite sign* in BEMB2 compared to BEMB1. It can be seen from the contact distances given that whenever a given intermolecular contact involves a Br–Br or an Me–Me in BEMB2 the same contact in BEMB1 generally involves the opposite type of contact, *i.e.* a Br–Me or an Me–Br contact. For BEMB1 a negative correlation for site 66502 gives a reduction of the proportion of Me–Me and Br–Br contacts and a corresponding increase in the proportion of Me–Br contacts relative to a random distribution. For BEMB2 the same result is achieved by a positive correlation.

(iii) For the neighbours directly up the **b** axis, however, (i.e. sites 56501 and 54501) the numbers of different types of contact are the same in the two cases and it might be expected that correlation along this vector should be the same in the two compounds. However, even here the correlations are of opposite sign, although for BEMB1 the actual value is very small.

(iv) In both BEMB1 and BEMB2 the neighbour at 64501 is the third largest in magnitude even though this is a molecule which is not in direct contact with the central 55501 molecule. Again the signs of this correlation are opposite in the two compounds.

In the same way that the previous BEMB1 results could not be explained in terms of a simple interatomic interaction model involving either partial charges on the Br and Me substituents or local dipoles, the results for BEMB2 present similar difficulties. In both compounds, only for the interaction between the central 55501 molecule and that at 66502 (which involves only a single contact between the disordered atomic sites) does the simplistic view that energetically Br–Me contacts are preferred to Me–Me or Br–Br contacts correctly predict the sign of the observed correlation. For other neighbouring sites such as 65501 and 56501 which involve competing interactions, the same simplistic view cannot explain the observed effects. As was discussed for the case of BEMB1 it is perhaps not surprising that this simplistic view of molecular ordering is inadequate to explain in detail our observed values for $C_{n,m}$. It is well known that lattice-energy sums involving electrostatic interactions are slowly convergent and truncating the

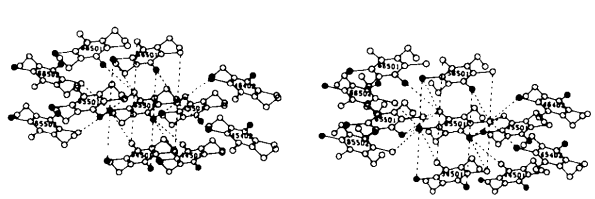

Fig. 3. A stereoscopic view of the molecular environment of the molecule at site 55501. All molecules shown are in orientation *A*. Dark atoms represent Br and light atoms are C.

summation at the first nearest neighbour is likely to lead to misleading results (see *e.g.* Kitaigorodskii, 1973, p. 144). Kitaigorodskii (1973, p. 160) has also pointed out that the main problem in obtaining lattice energies is not in computing the energy sums but in obtaining sufficient information regarding the charge distribution. In order to establish a more realistic model for the short-range order in molecular crystals such as BEMB1 and BEMB2, it appears necessary to try to establish a detailed description of the charge distribution over the whole molecule and carry out energy sums over a sufficiently large range of interaction distances. When this is done the present results, together with results from similar experiments, should be used to test such a theory.

5. Further considerations

The 'hole' in the diffuse scattering at the (010) reciprocal point is an extremely unusual and interesting phenomenon since it appears to represent a sort of 'space-group absence' in the diffuse scattering analogous to the systematic absence of the $k=2n+1$ Bragg peaks caused by the 2_1 axis. Extinctions in diffuse scattering intensities are not unusual when the disorder is of a *displacive* nature. For example, stacking faults in hexagonal close-packed structures give rise to an extinction along rows *hk* in reciprocal space such that $h-k=3n$ (n = integer), see p. 232 of Guinier (1963). For a purely substitutional type of disorder, extinctions may occur if the difference in the molecular scattering factors, $\Delta F = F_A - F_B$, is zero at some position in reciprocal space, either accidentally or as a result of symmetry relationships which may exist between *A* and *B*. In the present case such a simple explanation appears untenable because of the following considerations.

For the Bragg intensities, which are proportional to the square of the average molecular scattering factor, the systematic absence occurs because on average for every molecule with a coordinate of y along **b** there will be another related by the 2_1 axis at $y+\frac{1}{2}$, which will scatter exactly out of phase. On the other hand, for the diffuse scattering intensity there are four different terms which contribute for any pair of sites see (*e.g.* § 2.3 of Welberry, 1985). These correspond to the situations when the two sites are occupied by molecules in orientations *AA*, *AB*, *BA* or *BB*. Fig. 3 shows a stereoplot of the structure in which each of the molecules is depicted in orientation *A*. It is seen that the y coordinates of the molecules at for example 65502 are not simply related to those for 55501 by the addition of 0·5. However, if 55501 remains in orientation *A* while 65502 is changed to orientation *B* then the simple relation will hold. That is to say, *AB* and *BA* pairs locally preserve the 2_1 axis while *AA* or *BB* pairs destroy it. *AA* and *BB* pairs would therefore contribute to the intensity at the $0k0$, $k=2n+1$ positions but *AB* or *BA* pairs would not. Since in general we expect to have reasonably large proportions of each of the four pair types, the total contribution to the intensity will not be zero. This phenomenon is currently being investigated further and the results of these investigations will be reported elsewhere.

The discussion of the 'hole' given above and of the sharply peaked features observed in the ($0kl$) section given in § 3 suggests that some $C_{n,m}$ of a substantially high order (say ten cell spacings) must be significant in BEMB2. On the other hand, the least-squares analysis revealed that low-order correlations were fairly small. While this is not an impossibility it would certainly be rather unexpected and contrary to the predictions of many simple theoretical models of disorder. For example, if we consider the correlation field of near-neighbour interaction models such as the Ising model (see *e.g.* Montroll, Potts & Ward, 1963), the presence of low near-neighbour correlations necessarily results in very low correlations between distant neighbours. Conversely, if substantial correlations exist between distant neighbours then the near-neighbour correlations would be expected to be large also. In this light the diffuse scattering pattern of BEMB2 presents some unanswered questions and further work is required to explain fully the anomaly.

A possible explanation may be sought in terms of the fact that the present study made two basic assumptions which are not necessarily tenable in practice. Firstly, we assumed, as in all previous work, that the disorder is homogeneous. That is to say, that the statistical properties of the lattice are independent of position in the lattice. Secondly, we have assumed in this study (and in some previous similar studies) that the average symmetry of the lattice was $P2_1/c$ instead of $P2_1$ as given by the Bragg analysis. This second assumption means that the determined values of $C_{n,m}$ are in fact the average of two possibly different correlations which may exist along vectors which are symmetry related in $P2_1/c$ but unrelated in $P2_1$. Since the BEMB2 molecule is itself noncentrosymmetric it seems unlikely that the environment of a single site can become completely centrosymmetric as assumed by the present analysis. To resolve this problem it would be necessary to obtain much-higher-angle diffraction data, preferably at low temperature, in order to be able to distinguish the correlation distributions which our present experiment could not.

If we also take into account the possibility of inhomogeneity (*e.g.* different growth sectors of the crystal may exhibit differences in their correlation structure) then it is possible that each $C_{n,m}$ value should be considered to be the average of a larger number of different possible correlations. The degree of flexibility in the choice of individual correlation values which this would allow could perhaps account

for the significant high-order correlation effects while maintaining the small low-order values. At the present time, however, it must be stressed that such a possibility is merely conjecture.

Another possibility which is being investigated as an explanation for the occurrence of the 'hole' in the diffuse scattering is in terms of effects analogous to the 'atomic-size effect' which was first discussed by Warren, Averbach & Roberts (1951) for alloys. This takes account of the fact that a disordered distribution of two types of atoms will relax to alleviate strains caused by their different sizes, by allowing the atoms to shift from their idealized positions. These atomic displacements modify the ordinary substitutional disorder diffuse scattering both by redistributing the original scattering and also by producing additional effects. These effects may be taken account of in the case of alloys using analysis procedures described for example by Hawakawa, Bardhan & Cohen (1975). In particular we note that certain terms in the intensity expression given by these authors have a minimum in the region of Bragg positions. The fact that a molecule has rotational as well as translational degrees of freedom which may be utilized to alleviate size-effect strain means that for molecular crystals the analysis is necessarily considerably more complex than for alloys, and until such an analysis is made this explanation for the presence of the 'hole' cannot be tested.

We are grateful to K. Owen, M. Puza and G. Lockhart for technical assistance. One of us (JS) gratefully acknowledges the receipt of an Australian National University Scholarship during the tenure of which this work was carried out.

References

EPSTEIN, J. & WELBERRY, T. R. (1983). *Acta Cryst.* A**39**, 882-892.
GUINIER, A. (1963). *X-ray Diffraction.* San Francisco: Freeman.
HAWAKAWA, M., BARDHAN, P. & COHEN, J. B. (1975). *J. Appl. Cryst.* **8**, 87-95.
JOHNSON, C. K. (1976). *ORTEP*II. Report ORNL-5138. Oak Ridge National Laboratory, Tennessee.
KITAIGORODSKII, A. I. (1973). *Molecular Crystals and Molecules.* New York: Academic Press.
MONTROLL, E. W., POTTS, R. B. & WARD, J. C. (1963). *J. Math. Phys.* **4**, 308-322.
WARREN, B. E., AVERBACH, B. L. & ROBERTS, B. W. (1951). *J. Appl. Phys.* **22**, 1493-1496.
WELBERRY, T. R. (1983). *J. Appl. Cryst.* **16**, 192-197.
WELBERRY, T. R. (1985). *Rep. Prog. Phys.* **48**, 1543-1593.
WELBERRY, T. R. & GLAZER, A. M. (1985). *Acta Cryst.* A**41**, 394-399.
WELBERRY, T. R. & JONES, R. D. G. (1980). *J. Appl. Cryst.* **13**, 244-251.
WELBERRY, T. R. & SIRIPITAYANANON, J. (1986). *Acta Cryst.* B**42**, 262-272.
WOOD, R. A., TODE, G. E. & WELBERRY, T. R. (1985). *J. Appl. Cryst.* **18**, 371-372.
WOOD, R. A., WELBERRY, T. R. & PUZA, M. (1984). *Acta Cryst.* C**40**, 1255-1260.

Acta Cryst. (1987). B**43**, 106-110

A Revision of van der Waals Atomic Radii for Molecular Crystals. II: Hydrogen Bonded to Carbon

BY S. C. NYBURG, C. H. FAERMAN AND L. PRASAD

Department of Chemistry, University of Toronto, Toronto, Canada M5S 1A1

(*Received* 12 *March* 1986; *accepted* 11 *June* 1986)

Abstract

The neutron diffraction subset of the Cambridge Structural Database has been used to yield intermolecular non-bonded distances H···H, $d_{HH} \leq 3{\cdot}0$ Å, where hydrogen is bonded to carbon. For both sp^2-hybridized and sp^3-hybridized carbon, the non-bonded effective shape of the hydrogen atom appears to be that of a spheroid of revolution about the bond with the shortest radius towards the pole ('polar flattening'). For sp^3-hybridized carbon, the spheroid is centered on the proton; for sp^2-hybridized carbon, on the other hand, the center of the spheroid is 0·42 Å away from the proton towards carbon. The effective radii are shorter in this case than when hydrogen is bound to sp^3-hybridized carbon.

Introduction

Ever since Pauling's pioneering tabulations (1939) and revisions by others (*e.g.* Bondi, 1964), the non-bonded shape of a hydrogen atom in a crystal has been regarded as that of a sphere about the proton of van der Waals radius *ca.* 1·20 Å. Accordingly, it has become routine in crystal structure analysis to

0108-7681/87/010106-05$01.50